6-15-2009

Multimillion Atom Simulations with NEMO 3-D

Shaikh Ahmed
Purdue University - Main Campus

Neerav Kharche
Purdue University - Main Campus

Rajib Rahman
Purdue University - Main Campus

Muhammad Usman
Purdue University - Main Campus

Sunhee Lee
Purdue University - Main Campus

See next page for additional authors

Full-Band and Atomistic Simulation of Realistic 40 nm InAs HEMT

Mathieu Luisier, Neophytos Neophytou, Neerav Kharche, and Gerhard Klimeck
Network for Computational Nanotechnology and Birck Nanotechnology Center,
Purdue University, West Lafayette, IN 47907, USA; email: mluisier@purdue.edu

Abstract

A realistic 40 nm InAs high electron mobility transistor is studied using a two-dimensional, full-band, and atomistic Schrödinger-Poisson solver based on the $sp^3d^5s^*$ tight-binding model. Bandstructure non-parabolicity effects, strain, alloy disorder in the InGaAs and InAlAs barriers, as well as band-to-band tunneling in the transistor OFF-state are automatically included through the full-band atomistic model. The source and drain contact extensions are taken into account a posteriori by adding two series resistances to the device channel. The simulated current characteristics are compared to measured data and show a good quantitative agreement.

Introduction

The scaling properties of high electron mobility transistors (HEMTs) with III-V compound semiconductor channels are currently investigated by both industry and academia. The logic performance of InGaAs and InAs based HEMTs with a gate length and a multi-quantum-well channel thickness scaled down to 40 and 10 nm, respectively has been recently reported [1,2]. It is expected that such devices will profit from the very high mobility of InAs, 20,000 cm^2/Vs, to exhibit high-speed operation, low-power consumption, and to outperform the conventional Si devices.

The interest in physics-based computer design to develop novel technology such as InAs HEMTs has considerably increased in the last decade. However standard techniques such as drift-diffusion are not adapted to the nanoscale devices shown in Ref. [1] and [2]. In effect they cannot capture the strong confinement of the electrons and the resulting quantization of the energy levels. In order to remedy to this deficiency quantum mechanical treatments within the effective mass approximation have been recently proposed for III-V devices [3]. However, the non-parabolicity of the InAs lowest conduction band is missing so that the electron states cannot be correctly populated. At a higher level full-band simulations have also been attempted, but they are restricted to very small Si structures [4] (channel thickness of 3 nm, total length of less than 30 nm) or they are based on semi-classical one-dimensional approaches [5].

In this paper we present a highly-efficient ballistic, two-dimensional, full-band, atomistic, and quantum mechanical simulator [6,7] to study realistic InAs HETMs with InGaAs and InAlAs barriers as proposed in Ref. [2]. The tool is based on the nearest-neighbor $sp^3d^5s^*$ tight-binding model and a Wave Function approach, equivalent to the Non-Equilibrium Green's Function formalism, but computationally much more efficient in the case of ballistic transport. Its four levels of parallelism and its optimized numerical algorithms allow the simulation of 140 nm long devices with a channel thickness up to 12 nm [8]. This goes much beyond the capabilities of any other full-band atomistic simulator. Furthermore, quantitative agreement with the experimental data of Ref. [2] is obtained.

Approach

The computer-aided investigation of large devices such as the HEMT depicted in Fig. 1 requires the establishment of a three-level hierarchy of the simulation domain, one for the strain relaxation (entire structure), one for Poisson equation (region delimited by the black dashed line), and one for the quantum transport problem (shaded region).

The valence-force-field (VFF) method with a Keating potential is used to relax the atom positions in the channel [9]. Strain is caused by the InAs-InGaAs and InAs-InAlAs lattice mismatch. In effect $In_{0.53}Ga_{0.47}As$ has a lattice constant a_0 of 0.5868 nm (same as InP) so that the thin InAs layer grown on top of it (a_0=0.60583 nm) undergoes a biaxial compression. Since strain is a long range effect its calculation extends over a volume of 1,414,400 atoms, starting from the InP substrate while the atomistic transport domain contains 38,556 atoms.

The 2D Poisson equation is solved with the finite element method on a domain that includes the gate contact (Dirichlet) and whose electrical field vanishes at the other boundaries (Neumann). For computational reasons only 20 nm of the lower InAlAs layer are taken into account. Finally, we simulate the atomistic and full-band transport properties of the active region using the approach described in Ref. [6] and [7]. Electrons are injected into the device at different wave vector and energy values and the resulting contributions are summed up to give carrier and current densities. We consider each atom individually so that random alloy disorder is automatically taken into account. The $sp^3d^5s^*$ tight-binding parameters for InAs, GaAs, and AlAs are taken from Ref. [9] and [10]. Spin-orbit coupling and hole transport are neglected, except for the calculation of the band-to-band tunneling OFF-currents.

To model the source and drain extensions of the device we attach two series resistances R_S and R_D to the quantum transport domain as shown in Fig. 1. Hence, the electrons in the channel see an effectively reduced drain-to-source $\tilde{V}_{ids}$=$V_{ds}-(R_S+R_D)\cdot I_d$ and gate-to-source $\tilde{V}_{igs}$=$V_{gs}-R_S\cdot I_d$ voltages as compared to the externally applied V_{ds} and V_{gs}. The variable I_d represents the simulated drain current.

Results

The InAs HEMT shown in Fig. 1 is studied to illustrate the capabilities of our simulator. It is based on the device

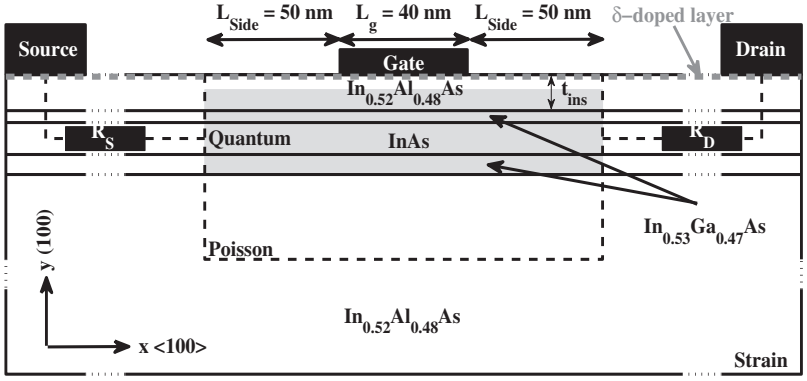

Fig. 1. Schematic view of the InAs HEMT. The 5 nm InAs quantum well is embedded between two $In_{0.53}Ga_{0.47}As$ layers (2 nm on top and 3 nm on the bottom). This active region is deposed on a thick $In_{0.52}Al_{0.48}As$ layer. A t_{ins}=4 nm thick $In_{0.52}Al_{0.48}As$ insulator layer separates the channel from the gate contact. The complete transistor structure shown here is used to calculate the strain profile caused by InAs-InGaAs lattice mismatch. Poisson equation is computed on the rectangular domain delimited by the dashed line. The quantum transport problem is solved in the gray area only. This region comprises the 10 nm InGaAs-InAs-InGaAs multi-quantum-well structure as well as half of the InAlAs top insulator so that the electron confinement is correctly reproduced. The gate length L_g measures 40 nm and L_{Side}=50 nm on the source and drain side is included in the transport calculation. A δ-doped layer (dashed gray line, n_{2D}=3e12 cm^{-2}) is placed just below the gate contact while the InAs channel is undoped. The source and drain extensions are modeled by two series resistances R_S and R_D, respectively. The in-plane axis (z) is assumed periodic (periodicity length L_z=0.5868 nm of one unit cell) and modeled with a momentum dependence (k_z) of the density-of-states and transmission coefficient.

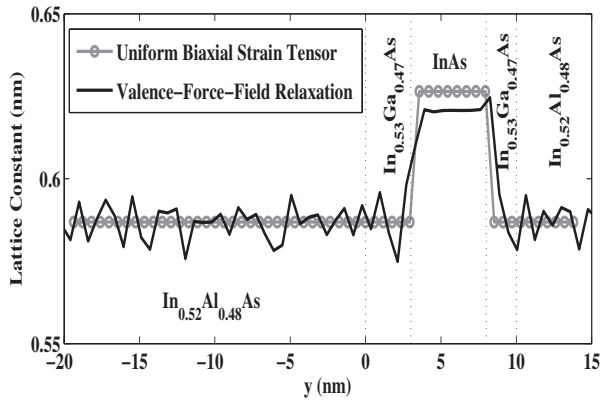

Fig. 2. Lattice constant along the y-axis (growth direction) in the middle of the gate contact. The black line represents the results obtained from the valence-force-field method [9] applied to the whole transistor structure depicted in Fig. 1. The gray line with circles refers to the ideal case where the biaxial strain induced by InGaAs-InAs lattice mismatch is modeled by a uniform tensor where ϵ_{xx}=ϵ_{zz}=(a_{InGaAs}-a_{InAs})/a_{InAs} and ϵ_{yy}=-2·$C_{12}/C_{11}\cdot\epsilon_{xx}$. The reference lattice constant is a_0=0.5868 nm (InP).

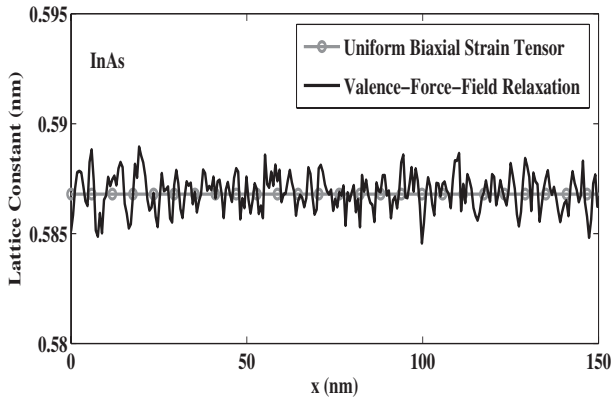

Fig. 3. Lattice constant along the x-axis in the middle of the InAs quantum well. The same conventions as in Fig. 2 are applied. The lattice constant of InAs in the plane parallel to the biaxial strain is compressed towards the $In_{0.53}Ga_{0.47}As$ value (0.5868 nm). In the plane orthogonal to the strain (Fig. 2) the lattice constant of InAs is extended by a factor (1+ϵ_{yy}) where ϵ_{yy}=0.034 in the present case. Note that the results from the uniform strain tensor agrees well with the VFF method.

of Ref. [2] with a gate length L_g of 40 nm, an insulator thickness t_{ins} of 4 nm, a source and drain injection region of 50 nm, and transport along the <100> crystal axis. The active region is composed of a $In_{0.53}Ga_{0.47}As$ (3 nm) - InAs (5 nm) - $In_{0.53}Ga_{0.47}As$ (2 nm) multi-quantum-well structure. To account for the penetration of the electrons into the upper $In_{0.52}Al_{0.48}As$ insulator 2 nm of this layer are included in the quantum mechanical calculation. In the transport direction 140 nm are simulated so that the full-band and atomistic region becomes a 12×140 nm^2 rectangular. The doping of the structure is realized with a delta-doped layer placed just below the gate contact and whose donor concentration is N_D=3e12 1/cm^2. The value of the source and drain series resistance is set to R_S=R_D=190 $\Omega\cdot\mu m$ to correctly reproduce the dI_d/dV_{ds} current slope at V_{gs}=0.4 V.

In Fig. 2 and 3 the lattice constants of the structure along the transport (x) and growth (y) directions are depicted. The relaxation of the atom positions is calculated either with the VFF method (black line) or assuming a uniform biaxial strain tensor (gray line with circles). As it can be observed in these two figures the uniform biaxial strain tensor is a good approximation along the transport direction, but fails to capture the correct relaxation of the atom positions along the growth direction.

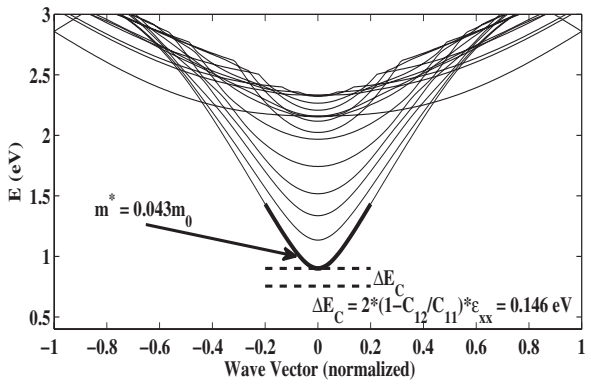

Fig. 4. Bandstructure (at k_z=0) of a 5 nm InAs quantum well embedded between $In_{0.53}Ga_{0.47}As$ barriers. It is used to describe the contacts and to inject states into the device. Due to the compressive strain and the electron confinement the conduction band edge of the InAs quantum well is pushed up in energy. Most of the current is carried by the lowest conduction subband whose effective mass m^* has a value of $0.043{\cdot}m_0$ due to the confinement along y (bulk: m^*=$0.023{\cdot}m_0$).

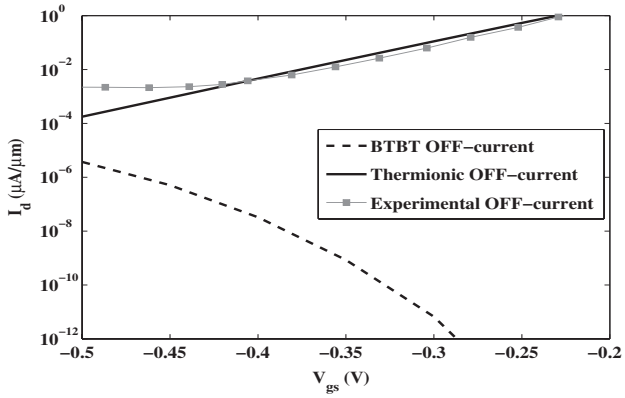

Fig. 5. Transfer characteristics $I_d - V_{gs}$ at V_{ds}=0.5 V and low V_{gs} of the 40 nm InAs HEMT depicted in Fig. 1. The simulated thermionic (black line) and band-to-band tunneling (BTBT, dashed line) currents are compared to the experimental OFF-current (gray line with squares). The latter is dominated by gate leakages and not by BTBT that is about 1-2 order of magnitude smaller at V_{gs}=-0.5 V. BTBT occurs between valence band electrons situated under the gate and conduction band electrons in the drain.

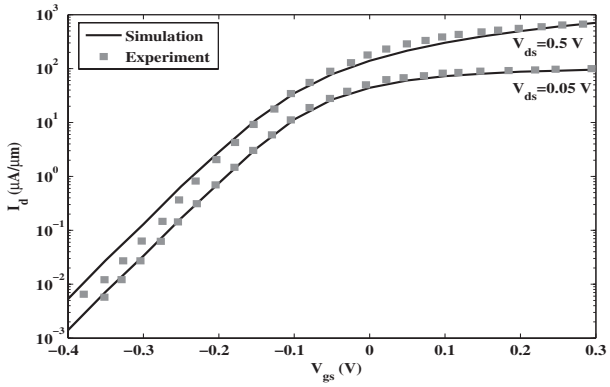

Fig. 6. Transfer characteristics $I_d - V_{gs}$ at V_{ds}=0.05 V and V_{ds}=0.5 V of the 40 nm InAs HEMT depicted in Fig. 1. The gray squares are experimental data [2] while the black lines are full-band and atomistic simulation results. The source and drain contacts are modeled by two series resistances of value R_S=R_D=190 $\Omega \cdot \mu m$.

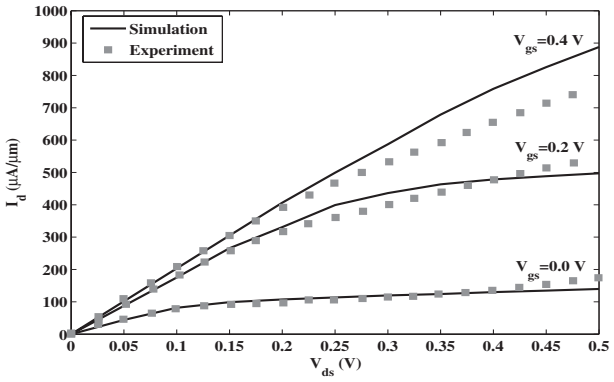

Fig. 7. Output characteristics $I_d - V_{ds}$ at V_{gs}=0.0 V, 0.2 V, and 0.4 V for the same 40 nm InAs HEMT structure as in Fig. 6. The gray squares refer to the experimental data of Ref. [2], the black lines to the simulation results performed in this work. The same R_S and R_D as in Fig. 6 are used.

The bandstructure of the multi-quantum-well active region is given in Fig. 4. Due to the compressive biaxial strain the conduction subbands are pushed to higher energy levels. At the same time and for the same reason the valence subbands (not shown here) are pushed down in energy. Hence, under the influence of strain and carrier confinement the effective band gap of the InGaAs - InAs - InGaAs structure is raised to about 0.77 eV, more than twice the bulk value of E_g=0.37 eV. Similarly, the effective mass of the lowest conduction subband increases from $0.024{\cdot}m_0$ (bulk) to $0.043{\cdot}m_0$ due to the finite thickness of the InAs body.

The larger electron effective mass and band gap are advantageous to manage the OFF-current of the device. In effect they induce a quasi suppression of band-to-band tunneling at low V_{gs} ($\leq$-0.2 V) and high V_{ds} (0.5 V). The OFF-current is mainly dominated by gate leakage (not considered here) and small thermionic emission. This is illustrated in Fig. 5 where the simulated thermionic and band-to-band tunneling currents are compared to the measurement of Ref. [2]. However, the maximum carrier velocity is proportional to $1/\sqrt{m^*}$ and therefore suffers from the effective mass increase as the ON-current. Note that the effective mass value is determined by the confinement of the electrons, and not by strain so that a thinner InAs layer gives a higher conduction band effective mass and a lower mobility limit.

Further comparisons between the experimental data from Ref. [2] and simulation results can be found in Fig. 6 to 8. Some of the most important transistor metrics like ON-current, threshold voltage, subthreshold swing, drain-induced barrier lowering, and transconductance maximum are summarized in Fig. 9. Good quantitative agreement is achieved for the transfer and output characteristics, except at high gate voltages where electron-phonon scattering may still play an important role. In Fig. 8 the slope of the simulated transconductance is

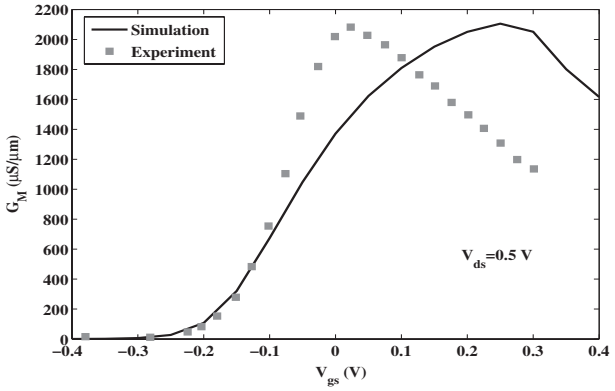

Fig. 8. Transconductance G_M vs V_{gs} at V_{ds}=0.5 V. The same InAs HEMT structure as in Fig. 6 and 7 is investigated. Experimental (gray squares) and full-band simulation results (solid line) are compared. The simulation results include the source and drain series resistances R_S and R_D (190 $\Omega \cdot \mu m$).

	Experiment	Simulation
V_{CC} (V)	0.5	0.5
I_{ON} at V_{gs}=0.3 V (μA/μm)	656	676
V_{th} (V)	-0.23	-0.23
S (mV/dec.)	70	72.7
$DIBL$ (mV/V)	80	96
G_{max} (μS/μm)	2083	2105
n_{2D} (1/cm^2)	2.9e12	2.9e12

Fig. 9. Performance parameters for the 40 nm InAs HEMT extracted from Fig. 6 to 8 and Ref. [2]. The experimental and simulated ON-current (I_{ON}), threshold voltage (V_{th}), subthreshold swing (S), $DIBL$, maximum of the transconductance (G_{max}), and channel electron density (n_{2D}) are given.

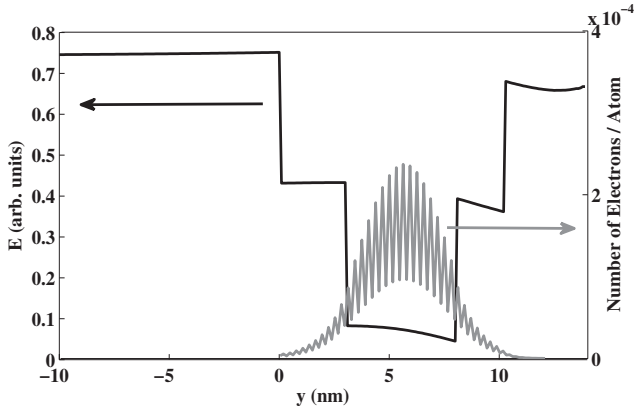

Fig. 10. Conduction band edge (black line) and number of free electrons per atom (gray line) along the y-axis at an external drain-to-source voltage V_{ds}=0.15 V and gate-to-source V_{gs}=0.15 V. The internal potentials $\tilde{V}_{ids}$ and $\tilde{V}_{igs}$ are equal to 0.05 and 0.1 V, respectively. The number of free electrons per cation (In, Ga, or Al) is lower than per anion (As).

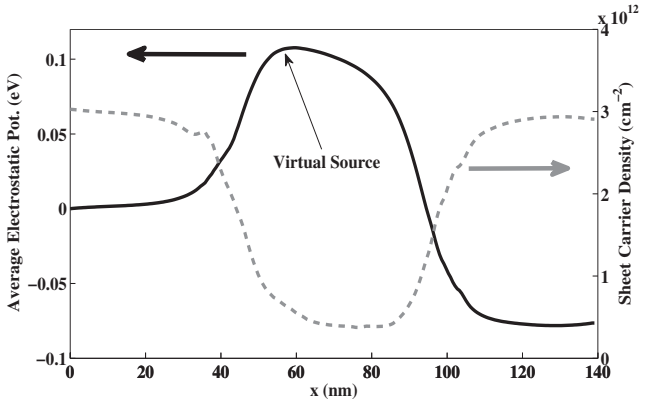

Fig. 11. Electrostatic potential (black line) and two-dimensional sheet carrier density(dashed gray line) along the transport x-axis at V_{ds}=0.15 V and V_{gs}=0.15 V ($\tilde{V}_{ids}$=0.05 V and $\tilde{V}_{igs}$=0.1 V). The maximum of the average electrostatic potential determines the position of the virtual source where the electron injection velocity is measured and calculated.

underestimated, but the maximum value matches the experiment. An exact knowledge of the HEMT structure as well as a better description of the source and drain contacts are necessary to improve the comparisons.

Finally, internal quantities such as the number of electrons, the conduction band edge, and the electrostatic potential along the x and y axis are presented in Fig. 10 and 11. As expected the electrons are confined in the InAs quantum well and slightly penetrate into the InGaAs barrier. From the plot of the electrostatic potential the position of the virtual source can be extracted, then the velocity of the carrier can be calculated ($v_{sim} \approx$ 3e7 cm/s), and compared to the measured value ($v_{meas} \approx$ 1.7e7 cm/s). The reason for this large discrepancy is unclear for the moment.

Conclusion

We have demonstrated in this paper the first multi-scale, full-band, and atomistic simulation of realistic 40 nm HEMT with quantitative agreement to experimental data. The tool has now been calibrated to study the scaling behavior of multi-quantum-well InAs channel down to 22 nm and below.

Acknowledgment

This work was partially supported by NSF grant EEC-0228390 that funds the Network for Computational Nanotechnology, by NSF PetaApps grant number 0749140, and by NSF through TeraGrid resources provided by the Texas Advanced Computer Center (TACC). Support by the Semiconductor Research Corporation (SRC) is acknowledged.

References

[1] D. H. Kim et al., IEDM 2006, p. 837. [2] D. H. Kim et al., IEDM 2007, p. 629. [3] K. Cantley, IEDM 2007, p. 113. [4] H. Minari et al., SISPAD 2007, p. 229. [5] A. Rahman et al., IEDM 2005, p. 601. [6] M. Luisier et al., Phys. Rev. B 74, 205323 (2006).[7] M. Luisier et al., SISPAD 2008. [8] G. Klimeck et al. IEDM 2008. [9] G. Klimeck et al., IEEE Trans. on Elec. Devices 54, 2079 (2007). [10] T. B. Boykin et al., Phys. Rev. B 66, 125207 (2002).